Carbohydrate Polymers 117 (2015) 106–114

Contents lists available at ScienceDirect

Carbohydrate Polymers

journal homepage: www.elsevier.com/locate/carbpol

Isolation and characterization of a hyperbranched proteoglycan from *Ganoderma Lucidum* for anti-diabetes

Deng Pan[a,1], Linqiang Wang[b,1], Congheng Chen[a], Bingwen Hu[b,*], Ping Zhou[a,*]

[a] State Key Laboratory of Molecular Engineering of Polymers, Department of Macromolecular Science, Fudan University, Shanghai 200433, PR China
[b] Shanghai Key Laboratory of Magnetic Resonance, Department of Physics, East China Normal University, Shanghai 200062, PR China

ARTICLE INFO

Article history:
Received 28 June 2013
Received in revised form 25 August 2014
Accepted 18 September 2014
Available online 28 September 2014

Keywords:
Ganoderma Lucidum
Structure characterization
Hyperbranched
Proteoglycan
Polysaccharide

ABSTRACT

Presently, an efficient protein tyrosine phosphatase 1B (PTP1B) inhibitor, named *FYGL-n*, was isolated from *Ganoderma Lucidum* and characterized for its structure and bioactivity. Structure and chain conformation of *FYGL-n* based on both chemical and spectroscopic analysis showed that *FYGL-n* was a hyperbranched heteropolysaccharide bonded with protein via both serine and threonine residues by O-type glycoside, and showed a sphere observed by AFM. Specifically, monosaccharide composition indicated that *FYGL-n* consisted of D-arabinose, D-galactose, L-rhamnose and D-glucose in a mole ratio of 0.08:0.21:0.24:0.47, with a molecular mass of 72.9 kDa. The analysis of amino acids in *FYGL-n* indicated that there were 16 common amino acids, among which aspartic acid, glycine, serine, alanine, glutamic acid and threonine were the dominant components. Also it was demonstrated that *FYGL-n* could inhibit the PTP1B activity on a competitive mechanism in vitro.

1. Introduction

Reversibility of protein phosphorylation is a predominant strategy to control the activity of proteins in eukaryotic cells. Approximately 30% proteins in the typical mammalian cells are thought to be phosphorylated (Szczepankiewicz et al., 2003). Tyrosine phosphorylation is considered to be a key reaction in the initiation and propagation of insulin action. Insulin exerts its physiological effects by binding to its receptor in insulin target tissues such as adipose, liver, and muscle. Insulin binding to the insulin receptor induces activation of the intrinsic tyrosine kinase in β-subunit, which serves as the first step in insulin signaling, and is followed by a cascade of intracellular events, such as glucose uptake (Kahn, 1994). There are compelling evidences that protein tyrosine phosphatase 1B (PTP1B) is primarily responsible for the dephosphorylation of insulin receptor, consequently, leading to the block of insulin signaling transduction pathway. Thus, an idea PTP1B inhibitor would be expected capable of increasing the half-life of the phosphorylated insulin receptor and enhancing the sensitivity of insulin (Kenner, Anyanwu, Olefsky, & Kusari, 1996). Such agents provide the promise as new therapies for the prevention and treatment of metabolic disorders, particularly for the treatment of diabetes which is considered to be one of the major leading causes of death in the world and currently affects more than 346 million people worldwide, with almost 3.4 million mortalities (Kim, Hyun, Choung, & Choung, 2006).

Nowadays the agents used for diabetes treatment mainly are synthetic drugs as well as insulin. However, these drugs usually come with considerable side effects, such as hypoglycemia, drug-resistance, dropsy and weight gain (Tahrani, Piya, Kennedy, & Barnett, 2010). Apart from those currently available therapeutic options for diabetes, herbal medicines have been recommended by World Health Organization (WHO) (Gupta & Mal, 2005). Herbal remedies are relatively effective, cheap and almost no side effects, compared to synthetic agents. One of examples is *Ganoderma lucidum* (*G. lucidum*), a white rot fungus, which has been widely used as a tonic in promoting longevity and health for thousands of years in China. Recently, a great deal of work has been carried out on this fungus, and demonstrated that some ingredients extracted from *G. lucidum* can promote the release of serum insulin and decrease the plasma glucose concentration in vivo (Huang et al., 2010; Trajkovic, Mijatovic, Maksimoviclvanic, & Stojanovic, 2009; Weng et al., 2009). Previously, we successfully isolated an efficient PTP1B inhibitor, named *FYGL*, from *G. lucidum* fruiting bodies (Teng et al., 2011). *FYGL* was an ingredient capable of decreasing

* Corresponding authors at: East China Normal University, Shanghai Key Laboratory of Magnetic Resonance, Department of Physics, Shanghai 200062, PR China. Tel.: +86 21 55664038; fax: +86 21 55664038.
E-mail addresses: bwhu@phy.ecnu.edu.cn (B. Hu), pingzhou@fudan.edu.cn (P. Zhou).
[1] These authors contributed equally to this work.

http://dx.doi.org/10.1016/j.carbpol.2014.09.051
0144-8617/

the plasma glucose level and enhancing the insulin sensitivity by inhibiting the activity and expression of PTP1B in vivo. We have already investigated the dominant components, inhibition kinetics, pharmacology and toxicity of the efficient extract in vivo, and demonstrated that *FYGL* can serve as a drug candidate or a healthcare food for the diabetic therapy or protection with high safety (Teng et al., 2011, 2012; Wang et al., 2012; Pan et al., 2013, 2014).

It is well known that the bioactivities of natural resources are dependent on their chemical structures and chain conformations (Liu et al., 2010; Tong et al., 2009; Sun, Liang, Zhang, Tong, & Liu, 2009). However, the structure information of *FYGL*, including molecular structure, residue linkages, branches, and morphology, etc., are still unclear due to the complexity of the natural resource. Therefore, in the present work, *FYGL* was further fractionated and structurally characterized for clarifying the structure–bioactivity relationship in detail. Herein, a neutral component, named *FYGL-n*, was fractionated from *FYGL*. The chemical structure of *FYGL-n* was investigated systematically by chemical and 2D NMR spectroscopic methods. The chain conformation of *FYGL-n* was also studied by dynamic and static light scattering method, and the structural parameters of *FYGL-n* were established based on the theory of polymer solution. Furthermore, *FYGL-n* inhibition kinetics on PTP1B activity was also evaluated in vitro. Hopefully, this work could provide valuable information on further understanding of the bioactive extracts from the natural resources.

2. Materials and methods

2.1. Materials

All the dried fruiting bodies of *G. lucidum*, grown in northeastern China, were purchased from Leiyunshang Pharmaceutical Co. Ltd. (Shanghai, China). Standard monosaccharide, DEAE-52 cellulose, Sephadex G-75, and Sephadex G-15 were bought from Whatman Co. (Shanghai, China). PTP1B was donated by Shanghai Viva Biotech Co. Ltd (Shanghai, China). *p*-Nitrophenyl phosphate (*p*-NPP), dimethyl sulfoxide (DMSO), methyl iodide (CH_3I) and methylbenzene from Sinopharm Co. Ltd. (Sichuan, China) were redistilled to remove trace water before use. Trifluoroacetic acid (TFA), sodium periodate ($NaIO_4$), sodium iodate ($NaIO_3$) and other necessary reagents from Sinopharm Co. Ltd. (Shanghai, China) were of analytical grade without further purification.

2.2. Preparation of FYGL-n

FYGL preparation procedures were based on a previous work (Teng et al., 2011). Briefly, after the dried fruiting bodies of *G. lucidum* were milled, defatted with boiling ethanol and decocted with boiling water, the solid residue was extracted with ammonia aqueous solution, and then the supernatant was neutralized, concentrated, dialyzed and lyophilized successively, and the crude extract was collected. Subsequently, the crude extract was further purified using Sephadex G-75 column (l.d. 80 × 26 cm) chromatography with 0.5 M NaCl solution as the eluent. The eluted fractions were monitored by the phenol–sulfuric acid method with ultraviolet (UV) absorption at wavelength of 490 nm, and the main fraction, named as *FYGL*, was obtained.

In the present work, *FYGL* was further fractionated using DEAE-52 column (l.d. 60 × 40 cm) with 0–0.3 M NaCl as eluent in a stepwise gradient manner. A neutral fraction, named as *FYGL-n*, was isolated from *FYGL*, and treated by Sevage agent (Staub, 1965) to remove free protein, and then dialyzed and lyophilized. The isolation process was carried out several times to obtain enough amounts for the analysis.

2.3. General analysis

Total contents of carbohydrate and uronic acid in *FYGL-n* were determined by colorimetric methods of phenol–sulphuric acid and *m*-hydroxydiphenol, using glucose and glucuronic acid as reference, respectively, (Blumencrantz & Hansen, 1973). Content of protein was determined by Lowry's methods with bovine serum albumin (BSA) as a standard (Bensadoun & Weinstein, 1976). UV absorption spectrum was recorded with a UV spectrophotometer (Model Lambda-35, Perkin Elmer, Massachusetts, USA).

2.4. Monosaccharide and amino acid component analysis

For monosaccharide analysis, *FYGL-n* (5 mg) was hydrolyzed with 2 M TFA (5 mL). The hydrolyzed product was reduced with $NaBH_4$, followed by acidification with 40% formic acid, and then the reduced sugars of alditols were acetylated with pyridine–acetic anhydride to produce the alditol acetates which were analyzed by gas chromatograph (GC, Tokyo, Japan). For absolute configuration analysis, a solution of 250 μL 0.625 M HCl in -(+)-2-butanol were added into the hydrolyzed product of *FYGL-n*, and kept at 80 °C for 16 h. The trimethylsilylated (TMS)-(+)-2-butyl glycoside-derivatives of monosaccharide were prepared with *N,O*-bis(tri-methylsilyl) trifluroacetamide (BSTFA) which were also analyzed by GC. For amino acids contents determination, the sample was vacuum-dried and placed in a hydrolysis vessel containing 18% HCl and 1% phenol. The vessel was purged with nitrogen gas and sealed under vacuum. The sample in the vessel was hydrolyzed at 110 °C for 24 h. After hydrolysis of the sample, the vessel was cooled and vacuum-dried to remove the residual HCl. The dried sample was dissolved in a citrate buffer of pH 2.2 and analyzed using a HitachiL-8500 amino acid analyzer packed with a cation exchange resin and eluted with a series of buffers ranging from low (0.25 M sodium citrate, pH 3.05) to high (0.25 M sodium nitrate, pH 9.5) pH values. Detection of amino acids was carried out using post-column derivatization with *o*-phthalaldehyde, a fluorescent reagent that reacts with all of the amino acids except proline. For praline detection, the sample was treated with sodium hypochlorite, and the same procedure as that used for other amino acid analysis was carried out.

2.5. Methylation, periodate oxidation and Smith degradation

In order to determine the glycosyl linkages, *FYGL-n* (5.0 mg) was methylated four times, using distilled DMSO and finely powdered dry NaOH. The vacuum-dried *FYGL-n* (5 mg) was dissolved in DMSO (1.5 mL) and then methylated with a saturated NaOH/DMSO solution (1.5 mL) and CH_3I (1 mL). The reaction mixture was extracted with chloroform, and the organic phase was washed with double-distilled water. Complete methylation was confirmed by the disappearance of —OH band (3200–3700 cm^{-1}) in FTIR spectrum. The permethylated *FYGL-n* was hydrolyzed, reduced and acetylated similarly as mentioned in Section 2.5. After those procedures, the methylated alditol acetates were re-dissolved in chloroform and analyzed using a gas chromatograph–mass spectrum (GC–MS, Shimadzu GC-14A, Tokyo, Japan).

Periodate oxidation and Smith degradation were performed to confirm the glycosidic linkages deduced from methylation analysis. *FYGL-n* was oxidized with 0.015 M sodium periodates at 4 °C in the dark. After the oxidation was completed, the solution was reduced, neutralized, dialyzed and lyophilized to give the polyalcohol which was then hydrolyzed and acetylated for GC analysis.

GC and GC–MS experiments were performed on a Shimadzu GC-14A gas chromatograph equipped with a DB-5MS column (30 m × 0.25 mm × 0.25 μm, Tokyo, Japan) and a flame ionization detector, using high purity of nitrogen as the carrier gas at a flow

rate of 8 cm^3/min. The temperature was heated up from 180 to 240 °C at 10 °C/min, and kept at 240 °C for 25 min. The vaporizer temperature was 260 °C and the detector temperature was 240 °C. A liquot (15 μL) was injected for each run.

2.6. Polysaccharide and protein linkages analysis

The linkages between polysaccharide and protein in *FYGL-n* were analyzed by the β-elimination reaction. *FYGL-n* were dissolved in 28% ammonium hydroxide aqueous solution saturated with ammonium carbonate at 60 °C for 40 h, and subsequently scanned by a UV spectrophotometer from 220 to 400 nm. Furthermore, 0.5 M boric acid was added into the reaction mixture which was then incubated at 37 °C for 30 min. After those procedures, the reaction product was desalted by Sephadex G-15 column (l.d. 5 cm × 1 cm), and subjected to the amino acid analysis. The linkage bonds between polysaccharide and protein in *FYGL-n* were determined by comparison with the amino acid contents in *FYGL-n* and the β-eliminated sample.

2.7. NMR characterization

All NMR experiments were recorded at 298 K on a Varian NMR System 700 spectrometer using a 5 mm [^{1}H, ^{13}C, ^{15}N]-triple resonance probe, with ^{1}H and ^{13}C π/2 pulses of 9 and 12.0 μs, respectively. ^{1}H NMR of *FYGL-n* was acquired by suppressing H_2O signal using WET (Water suppression Enhanced by T_1 effects) pulse sequence (Smallcombe, Patt, & Keifer, 1995). ^{13}C NMR and 2D NMR spectra (COSY, TOCSY, NOESY, HSQC and HMBC) of *FYGL-n* in D_2O solution were recorded at 298 K using TSP (3-(trimethylsilyl)-propionic acid-d_4 sodium salt) as an external standard. The relaxation delay for the NMR experiments was 1.5 s. The NOESY spectrum was recorded with a mixing time of 100 ms and TOCSY spectrum with a mixing time of 110 ms.

2.8. Fractionation of FYGL-n on different molecular weight

To determine the molecular parameters, it is necessary to fractionate *FYGL-n* on different molecular weight by the non-solvent addition method. Briefly, *FYGL-n* was dissolved in distilled water, and then methanol was slowly added into the solution drop-wise with stirring at room temperature until the solution turned turbid. The turbid solution was then heated to 50 °C and kept for 2 h, and the turbidity was somewhat decreased. After cooled down to 25 °C and kept for 2 h, the turbid mixture was centrifuged at 10,000 rpm for 30 min and the precipitate was washed several times by methanol, resulting in the first fraction. Similarly, the supernatant was subjected to the next fractionation by adding more volumes of methanol. Seven fractions, designated as *F*1, *F*2, *F*3, *F*4, *F*5, *F*6 and *F*7 were thus obtained. Each fraction was dialyzed and lyophilized.

2.9. Measurement of intrinsic viscosity

The intrinsic viscosities [η] of *FYGL-n* and its fractions *F*1 to *F*7 in distilled water and DMSO were measured at 25 °C by Ubbelohde capillary viscometer. The effluent time of the solvent was longer than 120 s, so that the kinetic energy correction was negligible. Huggins and Kraemer equations (1) and (2) were used to estimate the [η] value.

$$\frac{\eta_{sp}}{c} = [\eta] + k_h[\eta]^2 c \quad (1)$$

$$\ln\frac{\eta_r}{c} = [\eta] + k_k[\eta]^2 c \quad (2)$$

where k_h and k_k are Huggins and Kraemer coefficients, η_{sp} is the reduced specific viscosity, and η_r is the relative viscosity. The intrinsic viscosity [η] is obtained from the intercept of both linear functions of η_{sp}/c vs. c and $\ln \eta_r/c$ vs. c.

2.10. Determination of molecular structural parameters

For determination of molecular parameters of *FYGL-n*, the multi-angle static laser-light scattering measurements (MALLS) were performed at 25 °C with the multi-angles at 30, 45, 60, 75, 90, 105, 120, 135, 150°. Weight averaged molecular mass (M_w) and gyration radius (R_g) for the studied polymers in dilute solution were calculated on the Zimm's method based on Rayleigh–Gans–Debye theory as Eq. (3)

$$\frac{Kc}{R_\theta} = \frac{1}{M_w}\left[1 + \frac{16\pi^2\eta^2}{3\lambda^2}R_g^2\ \sin^2\left(\frac{\theta}{2}\right)\right] + 2A_2c$$
$$K = \frac{4\pi^2 n^2}{N_A\lambda^4}\left(\frac{dn}{dc}\right)^2 \quad (3)$$

where N_A, n, θ, c, and λ are Avogadro number, solvent refractive index, observed angle, polymer concentration, and light wavelength in vacuum, respectively. Additionally, the refractive index increment (dn/dc) of the *FYGL-n* in distilled water was measured by a double-beam differential refractometer. A plot of $Kc/R_{\theta\to 0}$ vs. c and $Kc/R_{c\to 0}$ vs. $\sin^2(\theta/2)$ can be used to determine the parameter of M_w and R_g, respectively.

Hydrodynamic radiuses (R_h) were measured by a Zetasizer nanoparticle analyzer (Malvern Instruments Ltd., Malvern, U.K.) using dynamic light scattering (DLS) technique.

2.11. Morphology measurement

AFM images of *FYGL-n* were recorded on an atomic force microscope (Digital Instruments, USA). A drop of 10 μL *FYGL-n* solution at concentration of 1 μg/mL in distilled water was dropped onto the freshly cleaved mica substrate and dried for 1.5 h. The freshly prepared sample was mounted on AFM stage and imaged under atmosphere (25 °C, relative humidity of 40–50%) using tapping model. The image was recorded at 256 × 256 pixels.

2.12. PTP1B inhibition and its kinetics measurement

The inhibitory potency of *FYGL-n* on the PTP1B activity was evaluated according to the method described in the literature (Szczepankiewicz et al., 2003). Briefly, 50 μL 1 mM *p*-nitrophenyl phosphates (pNPP) reacted with 50 μL 100 μg/mL PTP1B in a tris-NaCl buffer solution (pH 8.0) with or without inhibitor (*FYGL-n*) at 37 °C for 30 min, and the enzyme reaction was terminated by 3 M NaOH. The amount of produced *p*-nitrophenol was measured by UV absorbance at wavelength of 405 nm. The IC_{50} values referred to the concentration of the inhibitor required to decrease the initial PTP1B activity by 50% were used to evaluate the inhibitory potency of the inhibitor.

For determining the inhibition kinetics, *FYGL-n* aqueous solution at different concentrations of 0.0 (control), 50.0, 75.0 μg/mL were individually added to the reaction mixtures of 50 μL, 100 μg/mL PTP1B enzyme and 1 mM *p*NPP. The inhibition kinetics mechanism was determined using the Lineweaver–Burk plot.

3. Results and discussion

3.1. General properties of FYGL-n

FYGL-n was light yellow powder. The analysis of total sugar and protein contents indicated that *FYGL-n* was composed of

Table 1
Monosaccharide and amino acid components in *FYGL-n* .

Components	Monosaccharid content (%)	Components	Amino acid contents (%)	Components	Amino acid contents (%)	Components	Amino acid contents (%)
Glucose	47.0	Asp	14.40	Gly	12.80	Arg	1.20
Arabinose	8.0	Thr	8.98	Ala	9.88	Lys	1.54
Rhamnose	24.0	Ser	10.20	Val	7.81	His	1.21
Galactose	21.0	Glu	9.04	Ile	5.00	Cys	0.39
		Phe	3.58	Leu	7.54	Met	0.15
		Pro	5.84	Tyr	0.43		

Asp, aspartic acid; Asn, asparagine; Gly, glycine; Glu, glutamic acid; Gln, glutamine; Ala, alanine; Ser, serine; Thr, threonine; Leu, lecine; Phe, phenylalanine; Val, valine; Pro, proline; Ile, isoleucine;Tyr, tyrosine; Arg, arginine; Lys,lsine; His, histidine; Cys, cysteine; Met, methionine.

approximate 82 ± 2% polysaccharide and 12 ± 2% protein. Moreover, no uronic acid was detected in *FYGL-n*. Therefore, it was suggested that *FYGL-n* was a proteoglycan, i.e. the proteins in *FYGL-n* were covalently bound to the polysaccharide since the free proteins were removed by the Sevage method.

For the monosaccharide analysis, *FYGL-n* was hydrolyzed, reduced and acetylated into alditol acetate derivatives. Four peaks are detected at 6.26, 7.25, 8.01 and 8.11 min in GC spectrum (Data in Supporting information Fig. S1). By comparison with monosaccharide references, it is concluded that *FYGL*-n is composed of arabinose, galactose, rhamnose and glucose, with a ratio of 0.08: 0.21: 0.24: 0.47 (Table 1). For absolute configuration analysis, *FYGL*-n was hydrolyzed and derivatizated into TMS-derivatives, using -(+)-2-butanol and *N,O*-bis(tri-methylsilyl) trifluroacetamide (BSTFA). By comparison with those TMS-derivatives of standard monosaccharides, it can be concluded that the configurations of all glycosyl residues in *FYGL-n* are in D-enantiomers except rhamnose in L-enantiomer. The analysis of amino acids in *FYGL-n* indicated that there were 16 natural amino acids including aspartic acid/asparagine (Asx, 14.40%), glycine (Gly, 12.80%), serine (Ser, 10.20%), alanine (Ala, 9.88%), glutamic acid/glutamine (Glx, 9.04%), threonine (Thr, 8.98%), valine (Val, 7.81%), leucine (Leu, 7.54%), proline (Pro, 5.84%), isoleucine (Ile, 5.00%), phenylalanine (Phe, 3.58%), lysine (Lys,1.54%), histidine (His, 1.21%), arginine (Arg, 1.20%), tyrosine (Tyr, 0.43%), cysteine (Cys, 0.39%) and methionine (Met, 0.15%). The high contents of serine (10.2%) and threonine (8.98%) implied the possible existence of *O*-glycosidic linkage between polysaccharide and protein in *FYGL-n* (Chen, Xie, Nie, Li, & Wang, 2008).

3.2. Linkage features of FYGL-n

As demonstrated by methylation analysis, there were at least eleven types of linkages present in *FYGL-n* (Table 2 and supporting information Fig. S2). Specifically, the analytical results revealed that *FYGL-n* contained terminal residues of 2,3,4,6-Me_4-Glcp (8.18%), 2,3,4,6-Me_4-Galp (4.49%), 2,3,5-Me_3-Araf (2.93%), branched residues of 2,4-Me_2-Galp (11.15%), 3,6-Me_2-Glalp (9.38%), 6-Me-Glcp (19.1%), 3-Me-Rhap (5.69%), and remaining backbone residues of 2,3,6-Me_3-Glcp (2.97%), 2,3,4-Me_3-Galp (2.34%), 3,4-Me_2-Rhap (4.96%), 2,3,4-Me_3-Glcp (28.8%). Thus, the degree of branching (DB) could be calculated on the following equation:

$$DB = \frac{N_T + N_B}{N_T + N_B + N_L} \quad (4)$$

where N_T, N_B, and N_L are the total contents of the terminal residues (15.6%), branched residues (45.3%), and backbone residues (39.1%), respectively. The *DB* value of *FYGL-n* was thus calculated to be 0.61, implying a highly branched biomacromolecule (Aulenta & Hayes, 2003).

Periodate oxidation and Smith degradation of *FYGL-n* were performed to confirm the glycosidic linkages deduced from the methylation analysis. The residue products from periodate oxidation and Smith degradation of *FYGL-n* contained glycerol, rhamnose, erythrose, glucose and galactose in the GC spectrum (Supporting information Fig. S3). Large amount of the glycerol production implied that there might exist many glycosyl linkages, such as 1→, 1 → 2, 1 → 6 or 1 → 2,6, which could be attributed to the residues of 2,3,4,6-Me_4-Glcp, 2,3,4-Me_3-Galp, 2,3,4,6-Me_4-Galp, 3,4-Me_2-Rhap, and 2,3,5-Me_3-Araf, as characterized by methylation analysis (Liu & Sun, 2011). Similarly, the production of erythrose indicated that there might exist glycosyl linkage of 1 → 4 or 1 → 4,6 which could be assigned to 2,3,6-Me_3-Glcp (Askera & Shawky, 2010). The presences of glucose, galactose and rhamnose suggested that there were part of those monosaccharide linked in the form of 1 → 3, 1 → 2,3, 1 → 2,4, 1 → 3,4, 1 → 3,6 or 1 → 2,3,4, which might be attributed to 2,4,6-Me_3-Glcp, 3,6-Me_2-Galp, 2,4-Me_2-Galp or 6-Me-Glcp, respectively (Chandra, Ghosh, Ojha, & Islam, 2009). The results of periodate oxidation and Smith degradation well agreed with those of methylation analysis.

Linkage bonds between polysaccharide moiety and protein one in the proteoglycan can be classified into two types on the basis of their stability against alkali, one is *O*-glycosidic linkage, and the other is *N*-glycosidic linkage (Tao, Zhang, & Zhang, 2009). The alkali-sensitive *O*-glycosidic linkages (involving serine and threonine residues) can be easily broken in relatively mild condition by β-elimination reaction resulting in the release of the carbohydrate moiety, and the serine and threonine residues linked to hydroxyl of

Table 2
GC–MS analysis of methylated *FYGL-n*.

Peak no. in GC	MS fragments (*m*/*z*)	Methylated monosaccharide	Glycosidic linkage	Mole ratio (%)
1	43,87,101,117,129,161	2,3,6-Me_3-Glcp	→4)-Glcp-(1→	2.97
2	43,58,71,87,101,117,129,161,189,233	2,3,4-Me_3-Galp	→6)-Galp-(1→	2.34
3	43,101,71,75,88,99,143,175,102,222,115	2,3,4,6-Me_4-Glcp	Glcp-1→	8.18
4	43,59,71,87,101,117,129,145,161,205	2,3,4,6-Me_4-Galp	Galp-1→	4.49
5	43,131,129,89,87,117,189,99,113	3,4-Me_2-Rhap	→2)-Rhap-(1→	4.96
6	43,117,129,189,87,159,233	2,4-Me_2-Galp	→3,6)-Galp-(1→	11.15
7	43,117,190,233	3,6-Me_2-Galp	→2,4)-Galp-(1→	9.38
8	117,129,101,45,161,87,71,145	2,3,5-Me3-Araf	Araf-(1→	2.93
9	43,73,85,103,115,127,145,175,187,217	6-Me-Glcp	→2,3,4)-Glcp-(1→	19.1
10	43,129,143,87,117,189,101,203	3-Me-Rhap	→2,4)-Rhap-(1→	5.69
11	58,97,87,129,143,59,71,75,85,171,103,111,145,203	2,3,4-Me_3-Glcp	→6)-Glcp-(1	28.8

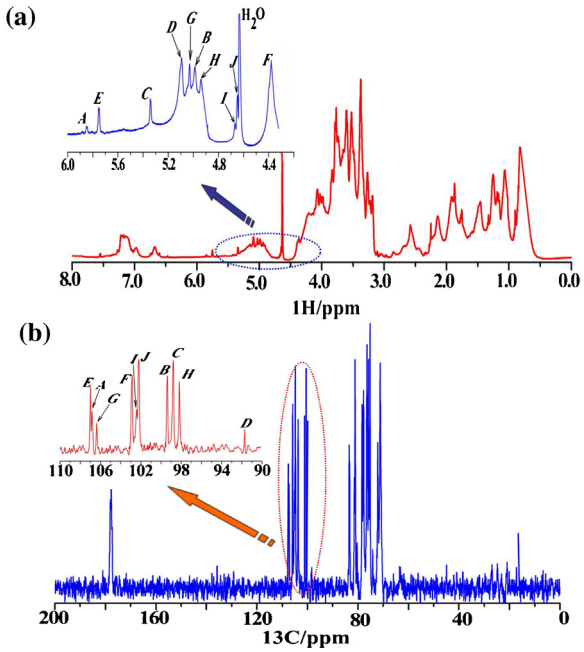

Fig. 1. ^{1}H NMR (a) and ^{13}C NMR (b) spectra of *FYGL-n* in D_2O solution; δ_H 4.65 is attributed to the trace H_2O.

the polysaccharide would be transformed to α-amino acrylic and α-amino butenoic acid, respectively, which have strong absorbance at 245 nm in UV spectrum. Furthermore, when the β-eliminated products were reduced and hydrolyzed, the contents of serine and threonine in the studied sample would be decreased while those of alanine and α-amino butyric acid would increase. UV spectrum of the alkali-treated *FYGL-n* (supporting information Fig. S4) showed a strong absorbance at 245 nm, implying that the β-elimination reaction took place and the α-amino acrylic or α-amino butenoic acid were formed. Moreover, after the β-eliminated products were reduced and hydrolyzed, the serine and threonine contents were drastically decreased from 8.98% and 10.2% to 5.00% and 6.40%, respectively, while the alanine content was increased from 9.88% to 12.1% (Supporting information Fig. S5 and T1). The results confirmed that the polysaccharides in *FYGL-n* were covalently linked to the protein in *O*-linkage type via both serine and threonine residues.

3.3. NMR characterization of FYGL-n

The chemical structure of *FYGL-n* was also characterized by one- and two-dimensional NMR. As shown in ^{1}H NMR (Fig. 1a), ^{1}H signals at δ_H 5.85, 5.75, 5.34, 5.09, 5.03, 4.99, 4.94, 4.65 and 4.39 ppm in the anomeric area further confirmed the heteropolysaccharide of *FYGL-n*. As shown in ^{13}C NMR (Fig. 1b), seven ^{13}C signals at δ_C 106.92, 106.85, 106.13, 99.68, 98.30, 98.04 and 91.97 ppm were observed in the anomeric area, also suggesting a heteropolysaccharide of *FYGL-n*. ^{13}C NMR signals at δ_C 170–175 ppm were assigned to the carbonyl groups, indicating the existence of protein (Chen et al., 2008). ^{1}H—^{13}C cross-peaks at $\delta_{H/C}$ 5.85/106.85, 4.99/99.68, 5.34/98.30, 5.09/91.79, 5.75/106.92, 4.39/102.50, 5.03/106.13, 4.94/98.04, 4.65/102.44 and 4.64/102.44 ppm, designated as ***A***, ***B***, ***C***, ***D***, ***E***, ***F***, ***G***, ***H***, ***I*** and ***J*** residues, observed in 2D HSQC NMR spectrum (Fig. 2a) indicated that the signals from carbons and protons in anomeric region were corresponded in each group pair, respectively.

^{1}H—^{1}H cross-peaks at $\delta_{H/H}$ 5.85/3.88, 3.88/4.08, 4.08/3.71, 3.71/4.23, 4.23/1.25 detected in ^{1}H—^{1}H COSY and ^{1}H—^{1}H TOCSY spectra (Fig. 2b and c) indicated that the signals of δ_H 5.85, 3.88, 4.08, 3.71, 4.23 and 1.25 corresponded to H-1 to H-6 of residue ***A***, respectively. Meanwhile the residue ***A*** had an anomeric chemical shifts larger than δ_H 5.0, and very small $^{3}J_{H\text{-}1,\ H\text{-}2}$ value (<3 Hz), suggesting the residue ***A*** being α-linked (Elizabeth, 1995). Based on the ^{1}H-^{13}C cross peak at $\delta_{H/C}$ 1.25/16.48 observed in HSQC spectrum (Fig. 2a), which was attributed to the methyl group (Marvelys, Maritza, Lilian, & Julio, 2006), it was concluded that residue ***A*** was α-L-rhamnose residues. Combined with proton signals from COSY and TOCSY spectra, the carbon signals in residue ***A*** were easily assigned from HSQC spectrum (Fig. 2a) as C-1 of δ_C 106.85, C-2 of δ_C 82.45, C-3 of δ_C 68.63, C-4 of δ_C 70.43, C-5 of δ_C 58.95 and C-6 of δ_C 16.48. The relatively downfield shifts of C-1 and C-2, referred to typical monosaccharide, indicated that those carbon atoms were substituted. Additionally, both ^{13}C chemical shifts of C-3 and C-5 smaller than 80 ppm indicated that the residue ***A*** was pyranose instead of furanose. Conclusively, residue ***A*** was suggested to be 1,2-linked α-L-rhamnose, identical to the result from chemical analysis. Similarly, according to NMR characteristics for *FYGL-n* as well as the standard monosaccharide, the residues from ***B*** to ***J*** were suggested to be 1,2,4-linked α-L-rhamnose, 1,3-linked α-D-glucose, 1-linked α-D-glucose, 1,2,3,4-linked α-D-glucose, 1,6-linked β-D-galactose, 1,2,4-linked α-D-galactose, 1,3,6-linked β-D-galactose, 1-linked β-D-galactose and 1,6-linked β-D-glucose, respectively. The complete carbon and proton signals of residues ***B*** to ***J*** were assigned similarly as that of residue ***A*** and summarized in Table 3. Furthermore, the signals of α, β and γ protons and carbons of the linked serine and threonine residues were also assigned in Table 3, according to the typical amino acid NMR.

^{1}H—^{13}C HMBC NMR spectrum, which could provide valuable information of ^{13}C—^{1}H three-bond coupling within intra-residue and the connection between residues through the glycosidic linkages, was applied to figure out the complete sequence of the residues in *FYGL-n*. Amounts of ^{1}H—^{13}C cross-peaks were observed in HMBC spectrum of *FYGL-n* (Fig. 2d). For instance, ^{1}H—^{13}C cross-peak at $\delta_{H/C}$ 5.85/69.41, denoted as **(1)** in HMBC spectrum, suggested the residue ***A*** of 1,2-linked α-L-rhamnose connecting the residue ***F*** of 1,6-linked β-D-glucose via 1 → 6 glycosidic linkage. Additionally, ^{1}H—^{13}C cross-peaks at $\delta_{H/C}$ 4.37/75.88 and 3.96/68.701, denoted as **(14)** and **(15)** in HMBC spectrum (Fig. 2d), respectively, suggested that the residues of threonine and serine were connected to the residues of 1,3-linked α-D-glucose and 1,6-linked β-D-glucose, identical to the conclusion in which the polysaccharides in *FYGL-n* were covalently linked to the protein in *O*-linkage type via both serine and threonine residues. Similarly, according to ^{1}H—^{13}C cross-peaks in HMBC spectrum as well as NOESY spectrum (Supporting information Fig. S6), the connections in the repeated units in *FYGL-n* were assigned systematically and summarized in Table 4. Therefore, the deduced hyperbranched chain sequence of *FYGL-n* was determined as Fig. 3 (detailed structure analysis in the Supporting information).

3.4. Molecular structural parameters of FYGL-n

According to the chemical structure as in Fig. 3, *FYGL-n* was considered to be highly branched. Thus, the molecular parameters, including intrinsic viscosity ($[\eta]$), gyration radius (R_g), hydrodynamic radius (R_h) and molecular mass (M_w) of *FYGL-n* in aqueous solution were also investigated using viscosity and light scattering methods. Good linear correlations of the plots of η_{sp}/c vs. c and $\ln\eta_r/c$ vs. c for *FYGL-n* in both distilled water and DMSO within concentration of 3–8 mg/mL at 25 °C (data in Supporting information Fig. S7a) suggested that *FYGL-n* was a neutral macromolecule instead of polyelectrolyte (Esquenet, Terech, Boué, & Buhler, 2004). By extrapolation of those two linear curves to the infinite dilution concentration, $[\eta]$ value of *FYGL-n* in distilled water and DMSO were determined as 20.6 mL/g. It was noted that there was no significant difference of $[\eta]$ of *FYGL-n* in both DMSO and water, implying that

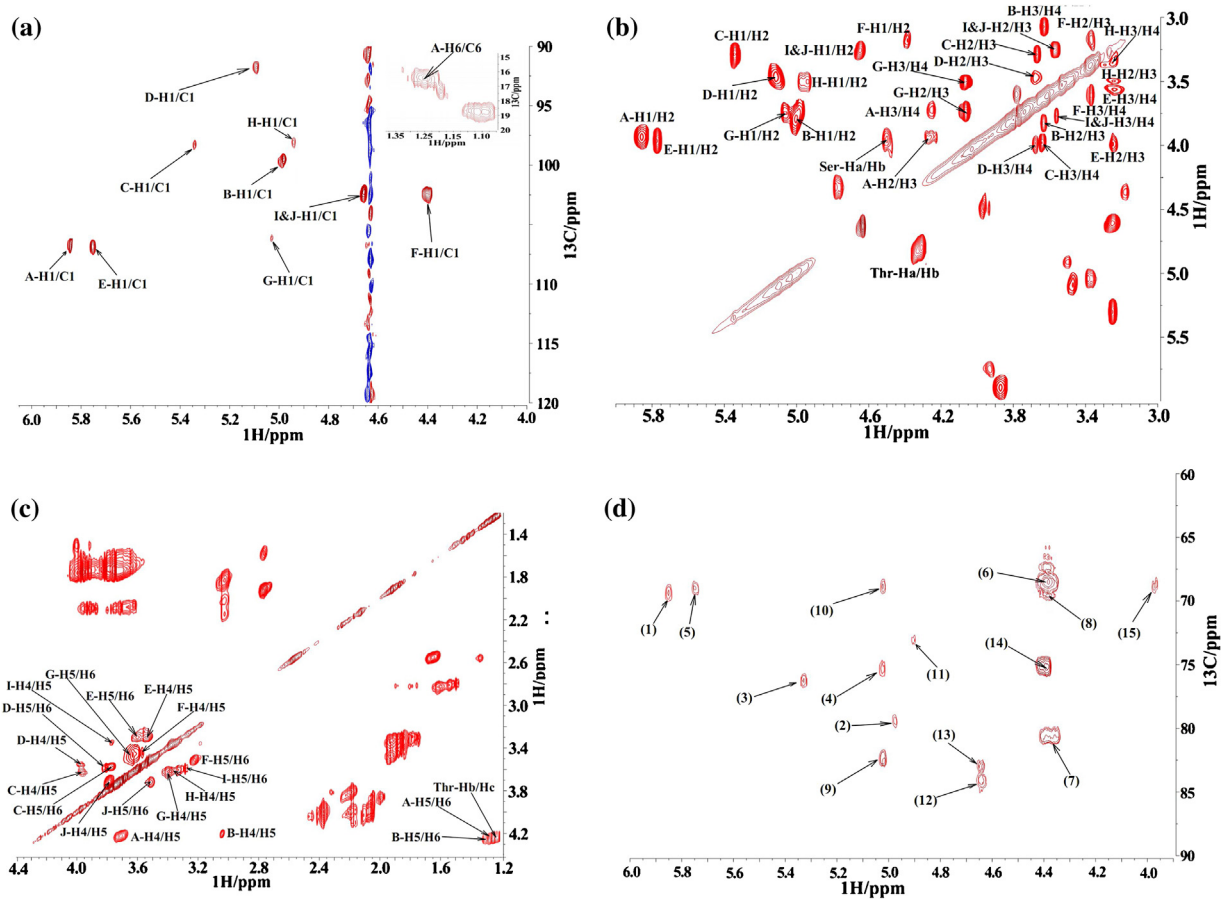

Fig. 2. 2D NMR spectra of anomeric groups in *FYGL-n* in D_2O. (a) $^1H—^{13}C$ HSQC; (b) $^1H—^{13}C$ HMBC; (c) $^1H—^1H$ COSY and (d) $^1H—^1H$ TOCSY NMR.

Table 3
Complete assignments (ppm) of ^1H and ^{13}C NMR of *FYGL-n*.

No.	Residues	$\delta_{H/C}$	$\delta_{H/C}$	$\delta_{H/C}$	$\delta_{H/C}$	$\delta_{H/C}$	$\delta_{H/C}$
A	→2)-α-L-Rhap-(1→	5.85/106.85	3.88/82.45	4.28/68.63	3.71/70.43	4.23/58.95	1.25/16.48
B	→2,4)-α-L-Rhap-(1→	4.99/99.68	3.78/75.34	3.62/71.26	3.08/82.21	4.23/88.95	1.26/16.48
C	→4)-α-D-Glcp-(1→	5.34/98.30	3.29/72.83	3.65/70.51	3.97/75.88	3.61/70.85	3.78/60.66
D	α-D-Glcp-1→	5.09/91.79	3.48/70.54	3.68/71.36	3.97/70.51	3.60/70.85	3.77/60.66
E	→2,3,4)-α-D-Glcp-(1→	5.75/106.92	3.92/79.07	3.24/73.13	3.55/80.64	3.31/72.50	3.60/60.59
F	→6)-β-D-Galp-1→	4.39/102.50	3.18/72.93	3.37/72.82	3.62/73.01	3.51/70.67	3.24/69.42
G	→2,4)-α-D-Galp-(1→	5.03/106.13	3.73/75.36	4.07/70.99	3.34/75.73	3.62/72.97	3.37/61.08
H	→3,6)-β-D-Galp-(1→	4.94/98.04	3.50/72.57	3.24/73.02	3.37/71.62	3.62/72.97	3.34/75.73
I	β-D-Galp-1→	4.65/102.44	3.26/72.96	3.55/72.81	3.77/73.05	3.34/69.49	3.58/62.64
J	→6)-β-D-Glcp-(1→	4.65/102.44	3.26/72.96	3.55/73.21	3.77/71.61	3.73/70.64	3.52/68.70
Thr	Threonine	4.32/61.88 (α)	4.37/73.38 (β)	1.23/17.0 (γ)	/	/	/
Ser	Serine	4.50/58.35 (α)	3.96/69.80 (β)	/	/	/	/

Table 4
$^{13}C—^1H$ connections of *FYGL-n* from HMBC NMR.

No.	Residues	$\delta_{H/C}$	$^{13}C—^1H$ Connections
A	→2)-α-L-Rhap-(1→	**(1)** 5.85/69.41	→2)-α-L-Rhap-(1→6)-β-D-Galp-1→
B	→2,4)-α-L-Rhap-(1→	**(2)** 4.99/79.08	→2,4)-α-L-Rhap-(1 → 4)-α-D-Glcp-(1,2,3→
C	→4)-α-D-Glcp-(1→	**(3)** 5.34/76.08	→4)-α-D-Glcp-(1 → 4)-α-D-Galp-(1,2→
D	α-D-Glcp-(1→	**(4)** 5.09/75.38	α-D-Glcp-(1 → 2)-α-D-Galp-(1,4→
E	→2,3,4)-α-D-Glcp-(1→	**(5)** 5.75/69.34	→2,3,4)-α-D-Glcp-(1 → 6)-β-D-Galp-(1,3→
F	→6)-β-D-Galp-(1→	**(6)** 4.39/68.6	→6)-β-D-Galp-(1 → 6)-β-D-Glcp-(1→
		(7) 4.39/80.63	→6)-β-D-Galp-(1 → 4)-α-D-Glcp-(1,2,3→
		(8) 4.39/69.42	→6)-β-D-Galp-(1 → 6)-β-D-Galp-(1→
G	→2,4)-α-D-Galp-(1→	**(9)** 5.03/82.23	→2,4)-α-D-Galp-(1 → 4)-α-L-Rhap-(1,2→
		(10) 5.03/68.72	→2,4)-α-D-Galp-(1 → 6)-β-D-Glcp-(1→
H	→3,6)-β-D-Galp-(1→	**(11)** 4.94/73.13	→3,6)-β-D-Galp-(1 → 3)-α-D-Glcp-(1,2,4→
I	β-D-Galp-(1→	**(12)** 4.65/75.27	β-D-Galp-(1 → 3)-β-D-Galp-(1,6→
J	→6)-β-D-Glcp-(1→	**(13)** 4.65/82.45	→6)-β-D-Glcp-(1 → 2)-α-L-Rhap-(1→
Thr	Threonine	**(14)** 4,37,75.88	Thr → 1)-α-D-Glcp-(3→
Ser	Serine	**(15)** 3.96,68.70	Ser → 6)-β-D-Glcp-(1→

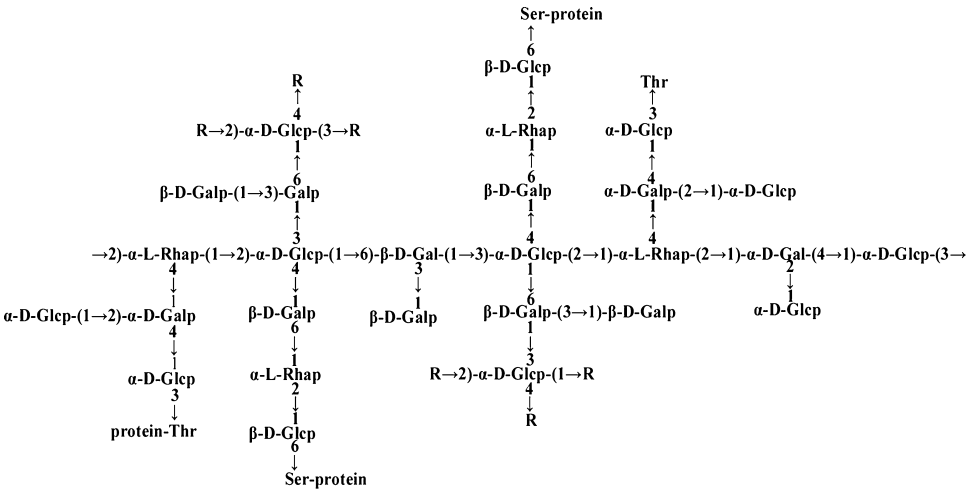

Fig. 3. Structure of *FYGL-n* based on chemical and NMR analysis. Rs represent the carbohydrate residues of →2,4)-α-L-Rhap-(1→, →6)-β-D-Galp-1→, Araf-(1→ or →3,6)-β-D-Galp-(1→.

FYGL-n molecule was an isolated polymer in both DMSO and water within such concentration range. Similarly, $[\eta]$ values of *F*1 to *F*5 in distilled water were also obtained (Supporting information Figs. S7b, S7c and T2).

The weight averaged molecular mass (M_w), the hydrodynamic radius (R_h) and the gyration radius (R_g) of *FYGL-n* and its fractions *F*1 to *F*7 were measured by dynamic and static laser-light scattering technology, indicating that *FYGL-n* was a macromolecule with weight averaged molecular mass (M_w) of 72.9 kDa (Supporting information Fig. S8 and T2).

The intrinsic viscosity of a polymer in solution is related to M_w on the Mark–Houwink equation (5):

$$[\eta] = kM_w^{\alpha} \tag{5}$$

The power value (α) of M_w in Mark–Houwink equation is dependent on shape and nature of the macromolecule in solution. Generally, α value of 0–0.5 suggests the shape of polymer being a dense sphere, and the value from 0.6 to 0.8 being a flexible chain, and the value greater than 1 being an elongated rod, while the value of 0 being a typical hard sphere (Ma, Zhang, Nishiyama, Marais, & Vignon, 2011). Therefore, the Mark–Houwink function was established by fitting the curve of $\lg[\eta]$ vs. $\lg M_w$ (plot in Supporting information Fig. S9a) as Eq. (6)

$$[\eta] = (0.178 \pm 0.12) M_w^{0.42\pm0.02} \tag{6}$$

The α value of 0.42 ± 0.02 suggests a sphere-like structure for *FYGL-n* in aqueous solution, i.e., a highly branched structure, identical to the results deduced from degree of branching (DB) and NMR analysis as above.

Moreover, the intrinsic viscosity can also be applied to evaluate the unperturbed dimension A ($A = (\langle r^2\rangle_0/M_w)^{1/2}$, where $\langle r^2\rangle_0$ is mean-square end-to-end distance) of a polymer by the intercept of plot of $[\eta]/{M_w}^{1/4}$ vs. ${M_w}^{1/2}$ on Zimm and Kilb theory as Eq. (7) which is more applicable for the hyperbranched polymer characterization.

$$\frac{[\eta]}{M_w^{1/4}} = K_0 + BM_w^{1/2}$$
$$K_0 = \Phi_0 \left(\frac{\langle r^2\rangle_0}{M_W}\right)^{3/2} \tag{7}$$

where Φ_0 is a constant of 2.87×10^{23} g/mL (Zimm and Kilb, 1959). Thus, a plot of $[\eta]/{M_w}^{1/4}$ vs. ${M_w}^{1/2}$ (plot in Supporting information Fig. S8b) was established on the following Zimm–Kilb equation:

$$\frac{[\eta]}{M_w^{1/4}} = 0.73 + 0.0024\ M_w^{1/2} \tag{8}$$

The unperturbed dimension of *A* value for *FYGL-n* was thus calculated from Eq. (8) to be 1.36 ± 0.15 Å which was close to that (1.48 Å) of the hyperbranched glycoprotein extracted from *sclerotia of regium* reported by Tao et al. (Tao, & Yan et al., 2007a; Tao, & Zhang et al., 2007b). Usually, the unperturbed dimension of a polymer is affected by the bond angle and the steric hindrance from both backbone and side chain. In general, a hyperbranched polymer has a Gaussian behavior with large unperturbed dimension because of its segments crowding each other in the vicinity of branching point (Tao & Xu, 2008). The unperturbed dimension value of *FYGL-n* much larger than that of the reported linear polymers was identical to the hyperbranched structure of *FYGL-n*, as shown in Fig. 3.

It is well-known that, for a given polymer solution, the ratio of the gyration radius to hydrodynamic radius, $\rho = R_g/R_h$, depends on the architecture and conformation of polymer chains. It has been reported that the ρ value for an extended stiff chain or rod like chain is higher than 2.0, such as the comb-branched polysaccharide, named AF1, extracted from *Auricularia auricula-judae* by Xu et al. with a ρ value of 2.3 in water (Xu, Xu, & Zhang, 2012). The ρ value from 1.5 to 1.7 indicates a flexible linear polymer in a good solvent; whereas the ρ value of 0.775 indicates a compact sphere (Nichifor, Lopes, Carpov, & Melo, 1999). For a hyperbranched structures, its theoretical ρ parameter was predicted as 1.22 on the hydrodynamic interaction according to the Kirkwood–Riseman pre-average approximation (Ioan, Aberle, & Burchard, 2000). The ρ parameter of *FYGL-n* was calculated to be 1.27 ± 0.06 by averaging ρ values of *F1* to *F7* (Supporting information Fig. S10 and T2), similar to that the reported hyperbranched polymers (Tao et al., 2007a,b; Lyulin, Adolf, & Davies, 2001; Burchard, Schmidt, & Stockmayer, 1980), suggesting that *FYGL-n* exhibits a hyperbranched macromolecule, probably as extendedly spherical particles in the aqueous solutions.

3.5. Molecular morphology

Molecular parameters of *FYGL-n* deduced from the polymer solution theory indicated that *FYGL-n* exist as a spherical chain conformation in aqueous solution. AFM is a powerful tool in

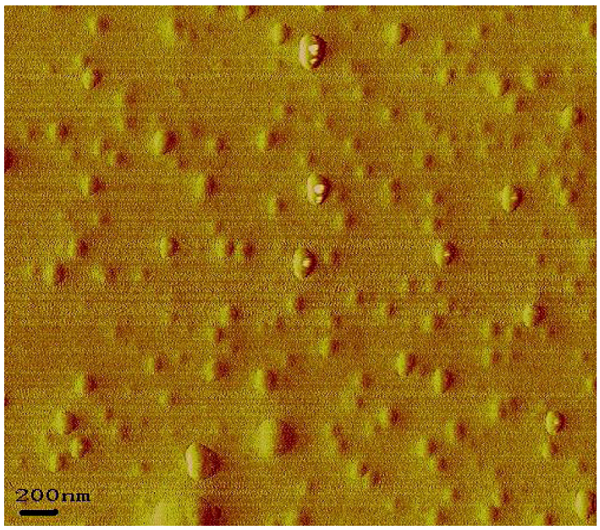

Fig. 4. AFM image of *FYGL-n* in distilled water at 25 °C.

investigating long chain-like molecule, such as polysaccharide, on the nanometer scale. Thus, to provide direct evidence of the chain conformation, AFM was used to observe the morphology in the present work. As shown in Fig. 4, the AFM image exhibits obviously globular particles in diameter within 150–200 nm, indicating that the *FYGL-n* molecules are dispersed individually in the extremely dilute solution. The globular particle sizes of *FYGL-n* in AFM image were identical to the hydrodynamic diameter (D_h) distribution measured by dynamic light scattering (Supporting information Fig. S11), supporting the hyperbranched structure of *FYGL-n* based on the polymer solution theory.

3.6. Inhibitory potency and interaction of FYGL-n on PTP1B

The inhibitory potency of *FYGL-n* on PTP1B activity in vitro was also investigated. IC_{50} value of *FYGL-n* on PTP1B was determined to be 7.8 ± 0.2 μg/mL. Meanwhile, the Lineweaver–Burk plots demonstrated that the inhibition mechanism of *FYGL-n* on PTP1B was typically competitive (Supporting information Fig. S12).

PTP1B is a ca. 50 kDa protein with highly polar phosphatase active sites surrounding protein surface, which is difficult to bind the lipophilic compound. PTP1B displays a substrate preference for phosphotyrosine flanked in the N-terminus by the acidic residues which positive active sites are likely to attract negatively charged substrates (Park, Bhattarai, Ham, & Cho, 2009). However, the significant negative charge substrates or agents are not always cell compatible in the drug development. Structure of PTP1B contains highly conserved WPD (tryptophan, proline, aspartic acid residues) loop and pTyr (tyrosine) loop (Barford, Flint, & Tonks, 1994). The WPD loop is flexible and in an 'open' conformation in the absence of its substrate, while closes once the pTyr loop binds the substrate. The key step during closure required for catalysis is the formation of hydrogen bond between the residue of Trp179 in the WPD loop and the residue of Arg221 in the pTyr loop (Kamerlin, Rucker, & Boresch, 2007). The extensive inter- and intra-molecular hydrogen bond donors and acceptors present in the hyperbranched biopolymer of *FYGL-n*. Some of the amino acid residues locating on the surface of *FYGL-n* might allow *FYGL-n* binding to the active sites in PTP1B competitively through hydrogen bonding and electrostatic interaction to prevent the interaction of PTP1B with its substrate. Meanwhile, the hyperbranched structure could maintain and stabilize the sphere-like conformation and its function (Seiler, Kohler, & Arlt, 2002). Thus, we preliminarily speculate that *FYGL-n* could block the pTyr loop in PTP1B binding to its substrate through hydrogen bonding, consequently keeping the WPD loop in open status, therefore deactivating the PTP1B. The detailed interaction mechanism of *FYGL-n* with PTP1B is still under investigation in our lab.

4. Conclusion

In summary, a highly water-soluble proteoglycan, *FYGL-n*, was isolated from *G. lucidum*. The present results demonstrated that *FYGL-n* was a hyperbranched heteropolysaccharide bonded with protein via both serine and threonine residues in *O*-type glycoside, and looked like a sphere in aqueous solution. The hyperbranched chain structure of *FYGL-n* may play special roles for its bioactivities of PTP1B inhibition and antihyperglycemic potency.

Acknowledgments

This work was supported by the NSFC (nos. 21074025, 21374022), Scientific Program of Shanghai Municipal Public Health Bureau (no. 2010231), Open Program of Shanghai Key Laboratory of Magnetic Resonance (no. 20101206), Science and Technology Innovation Program of k cjx.f (no. 11DZ1971802), Innovation Program of Shanghai Municipal Education Commission (no. 2012Z102460) and The Soft Science Program of Jing-An district in Shanghai (no. 2008RZ002). We also thank Dr. Min Xiao in Tennessee University for his assistance in article refinement

Appendix A. Supplementary data

Supplementary data associated with this article can be found, in the online version, at http://dx.doi.org/10.1016/j.carbpol.2014.09.051.

References

Askera, M. M. S., & Shawky, B. T. (2010). Structural characterization and antioxidant activity of an extracellular polysaccharide isolated from *Brevibacterium otitidis BTS 44*. *Food Chemistry*, *123*, 315–320.
Aulenta, F., & Hayes, W. (2003). Dendrimers: A new class of nanoscopic containers and delivery devices. *European Polymer Journal*, *39*, 1741–1771.
Barford, D., Flint, A. J., & Tonks, N. K. (1994). Crystal structure of human protein tyrosine phosphatase 1B. *Science*, *263*, 1397–1404.
Bensadoun, A., & Weinstein, D. (1976). Assay of proteins in the presence of interfering materials. *Analytical Biochemistry*, *70*, 241–250.
Blumencrantz, N., & Hansen, G. A. (1973). New method for quantitative determination of uronic acids. *Analytical Biochemistry*, *54*, 484–489.
Burchard, W., Schmidt, M., & Stockmayer, W. H. (1980). Information on polydispersity and branching from combined quasi-elastic and intergrated scattering. *Macromolecules*, *13*, 1265–1272.
Chandra, K., Ghosh, K., Ojha, A. K., & Islam, S. S. (2009). Chemical analysis of a polysaccharide of unripe (green) tomato (*Lycopersicon esculentum*). *Carbohydrate Research*, *344*(16), 2188–3194.
Chen, Y., Xie, M. Y., Nie, S. P., Li, C., & Wang, Y. X. (2008). Purification, composition analysis and antioxidant activity of a polysaccharide from the fruiting bodies of *Ganoderma atrum*. *Food Chemistry*, *107*, 231–241.
Elizabeth, F. H. (1995). ^{1}H NMR in the structural and conformational analysis of oligosaccharides and glycoconjugates. *Progress in Nuclear Magnetic Resonance Spectroscopy*, *27*, 445–474.
Esquenet, C., Terech, P., Boué, F., & Buhler, E. (2004). Structural and rheological properties of hydrophobically modified polysaccharide associative networks. *Langmuir*, *20*, 3583–3592.
Gupta, S., & Mal, M. (2005). Evaluation of hyperglycemia potential of *S. xanthocarpum* fruit in normal and streptozin induced diabetic rats. *European Bulletin Drugs Research*, *13*, 51–55.
Huang, C. Y., Chen, J. Y. F., Wu, J. E., Pu, Y. E., Liu, G. Y., & Pan, M. H. (2010). Ling-Zhi polysaccharides potentiates cytotoxic effects of anti-cancer drugs against drug-resistant urothelial carcinoma cells. *Journal of Agricultural Food Chemistry*, *58*, 8798–8805.
Ioan, C. E., Aberle, T., & Burchard, W. (2000). Structure properties of dextran. 2. Dilute solution. *Macromolecules*, *33*, 5730–5739.
Kahn, C. (1994). Insulin action, diabetogenes, and the cause of type II diabetes. *Diabetes*, *43*, 1066–1084.
Kamerlin, S. C. L., Rucker, R., & Boresch, S. (2007). A molecular dynamics study of WPD-loop flexibility in PTP1B. *Biochemical and Biophysical Research Communications*, *356*, 1011–1016.

Kenner, K. A., Anyanwu, E., Olefsky, J. M., & Kusari, J. (1996). Protein–tyrosine phosphatase 1B is a negative regulator of insulin- and insulin-like growth factor-I-stimulated signaling. *Journal of Biological Chemistry*, *271*, 19810–19816.

Kim, S. H., Hyun, S. H., Choung, S. Y., & Choung, S. Y. (2006). Anti-diabetic effect of cinnamon extract on blood glucose in db/db mice. *Journal of Ethnopharmacology*, *104*, 119–123.

Liu, C., Lu, J., Lu, L., Liu, Y., Wang, F., & Xiao, M. (2010). Isolation, structural characterization and immunological activity of anexopolysaccharide produced by *Bacillus licheniformis* 8-37-0-1. *Bioresource Technology*, *101*, 5528–5533.

Liu, J., & Sun, Y. (2011). Structural analysis of an alkali-extractable and water-soluble polysaccharide (ABP-AW1) from the fruiting bodies of *Agaricus blazei Murill*. *Carbohydrate Polymers*, *86*, 429–432.

Lyulin, A. V., Adolf, D. B., & Davies, G. R. (2001). Computer simulations of hyperbranched polymers in shear flows. *Macromolecules*, *34*, 3783–3789.

Ma, Z. C., Zhang, L., Nishiyama, Y., Marais, M. F., & Vignon, M. (2011). The molecular structure and solution conformation of an acidic heteropolysaccharide from *Auricularia auricula-judae*. *Biopolymers*, *95*, 217–227.

Marvelys, L., Maritza, M., Lilian, S., & Julio, H. (2006). Structural elucidation of the polysaccharide from *Sterculia apetala* gum by a combination of chemical methods and NMR spectroscopy. *Food Hydrocolloids*, *20*, 908–913.

Nichifor, M., Lopes, A., Carpov, A., & Melo, E. (1999). Aggregation in water of dextran hydrophobically modified with bile acids. *Macromolecules*, *32*, 7078–7085.

Pan, D., Zhang, D., Wu, J., Chen, C., Xu, Z., Yang, H., et al. (2014). A Novel proteoglycan from *Ganoderma Lucidum* fruiting bodies protects kidney function and ameliorates diabetic nephropathy via its antioxidant activity in C57BL/6 db/db Mice. *Food and Chemical Toxicology*, *63*, 111–118.

Pan, D., Zhang, D., Wu, J., Chen, C., Xu, Z., Yang, H., et al. (2013). Antidiabetic, antihyperlipidemic and antioxidant activities of a novel proteoglycan from *Ganoderma Lucidum* fruiting bodies on db/db mice and the possible mechanism. *PLoS One*, *8*(7), e68332.

Park, H., Bhattarai, B. R., Ham, S. W., & Cho, H. (2009). Structure-based virtual screening approach to identify novel classes of PTP1B inhibitors. *The European Journal of Medicinal Chemistry*, *44*, 3280–3284.

Seiler, M., Kohler, D., & Arlt, W. (2002). Hyperbranched polymers: new selective solvents for extractive distillation and solvent extraction. *Separation and Purification Technology*, *29*, 245–263.

Smallcombe, S. H., Patt, S. L., & Keifer, P. A. (1995). WET solvent suppression and its applications to LC NMR and high-resolution NMR spectroscopy. *Journal of Magnetic Resonance*, *117A*, 295–303.

Staub, M. A. (1965). Removal of proteins: Sevag method. *Methods in Carbohydrate Chemistry*, *5*, 5–6.

Sun, Y., Liang, H., Zhang, X., Tong, H., & Liu, J. (2009). Structural elucidation and immunological activity of apolysaccharide from the fruiting body of *Armillaria mellea*. *Bioresource Technology*, *100*, 1860–1863.

Szczepankiewicz, B. G., Liu, G., Hajduk, P. J., Cele, A. Z., Pei, Z., Xin, Z., et al. (2003). Discovery of a potent, selective protein tyrosine phosphatase 1B inhibitor using a linked-fragment strategy. *Journal of American Chemical Society*, *125*, 4087–4096.

Tahrani, A. A., Piya, M. K., Kennedy, A., & Barnett, A. H. (2010). Glycogenic control in type 2 diabetes: Targets and new therapies. *Pharmacology & Therapeutics*, *125*, 328–336.

Tao, Y., & Xu, W. (2008). Microwave-assisted solubilization and solution properties of hyperbranched polysaccharide. *Carbohydrate Research*, *344*, 3071–3078.

Tao, Y., Yan, F., & Zhang, L. (2007). Fractionation and characterization of a protein-polysaccharide complex from *Pleurotus tuberregium sclerotia*. *Journal of Polymer Science: Polymer Physics*, *45*, 2546–2554.

Tao, Y., Zhang, L., Yan, F., & Wu, X. (2007). Chain conformation of water-insoluble hyperbranched polysaccharide from fungus. *Biomacromolecules*, *8*, 2321–2328.

Tao, Y., Zhang, Y., & Zhang, L. (2009). Chemical modification and antitumor activities of two polysaccharide–protein complexes from Pleurotus tuber-regium. *International Journal of Biological Macromolecules*, *45*, 109–115.

Teng, B. S., Wang, C. D., Yang, H. J., Wu, J. S., Zhang, D., Zheng Fan, Z. H., et al. (2011). A protein tyrosine phosphatase 1B activity inhibitor from the fruiting bodies of *Ganoderma lucidum* (Fr.) Karst and Its hypoglycemic potency on streptozotocin-induced type 2 diabetic mice. *Journal of Agricultural and Food Chemistry*, *59*, 6492–6500.

Teng, B. S., Wang, C. D., Zhang, D., Wu, J. S., Pan, D., Pan, L., et al. (2012). Hypoglycemic effect and mechanism of a proteoglycan from *Ganoderma Lucidum* on streptozotocin-induced type 2 diabetic rats. *European Review for Medical and Pharmacological Sciences*, *16*, 166–175.

Tong, H., Xia, F., Feng, K., Sun, G., Gao, X., Sun, L., et al. (2009). Structural characterization and in vitro antitumor activity of a novel polysaccharide isolated from the fruiting bodies of *Pleurotus ostreatus*. *Bioresource Technology*, *100*, 1682–1686.

Trajkovic, L. M. H., Mijatovic, S. A., Maksimoviclvanic, D. D., & Stojanovic, M. B. (2009). Tufegdzic, S. J. Anticancer properties of *Ganoderma lucidum* methanol extracts *in vitro* and *in vivo*. *Nutrition and Cancer*, *61*, 696–707.

Weng, C. J., Chau, C. F., Yen, G. C., Liao, J. W., Chen, D. H., & Chen, K. D. (2009). Inhibitory effects of *Ganoderma lucidum* on tumorigenesis and metastasis of human hepatoma cells in cells and animal models. *Journal of Agricultural and Food Chemistry*, *57*, 5049–5057.

Wang, C. D., Teng, B. S., He, Y. M., Wu, J. S., Pan, D., Pan, L., et al. (2012). Effect of a novel proteoglycan PTP1B inhibitor from *Ganoderma Lucidum* on amelioration of hyperglycemia and dyslipidemia in db/db mice. *British Journal of Nutrition*, *108*, 2014–2025.

Xu, S., Xu, X., & Zhang, L. (2012). Branching structure and chain conformation of water-soluble glucan extracted from *Auricularia auricula-judae*. *Journal of Agricultural and Food Chemistry*, *60*, 3498–3506.

Zimm, B. H., & Kilb, R. W. (1959). Dynamics of branched polymer molecules in dilute solution. *Journal of Polymer Science*, *37*, 19–42.